Quaternary Science Reviews 201 (2018) 380–395

Contents lists available at ScienceDirect

Quaternary Science Reviews

journal homepage: www.elsevier.com/locate/quascirev

Late Holocene paleoseismology of Shuyak Island, Alaska

Ian Shennan [a, *], Martin D. Brader [a], Natasha L.M. Barlow [b], Frank P. Davies [a], Chris Longley [a], Neil Tunstall [a]

[a] Sea-Level Research Unit, Department of Geography, Durham University, Durham DH1 3LE, UK
[b] School of Earth and Environment, University of Leeds, Leeds LS2 9JT, UK

ARTICLE INFO

Article history:
Received 5 July 2018
Received in revised form
16 October 2018
Accepted 19 October 2018

ABSTRACT

We report stratigraphic evidence of land-level changes along the eastern portion of the Alaska-Aleutian megathrust. Four marshes on Shuyak Island record variable amounts of coseismic deformation during four pre-20th century earthquakes. We combine these data with paleoseismic evidence from across the Kodiak, Kenai and Prince William Sound segments of the megathrust. These indicate that in the last 2000 years, AD 1964 was the only one to rupture all three segments simultaneously and generate a M_w 9.2 earthquake. The Kodiak segment ruptured independently on four further occasions with magnitudes > M_w 8.0; in AD 1788 and c.400 (440–320) BP, and independently but around the times of great earthquakes in the Prince William Sound segment c.850 and c.1500 BP.

1. Context and aims

Paleoseismic information from coastal regions adjacent to subduction zones has the potential to characterise active earthquake sources for use in updating both seismic (Mueller et al., 2015; Wesson et al., 2007, 2008) and tsunami hazard maps (Nicolsky et al., 2013, 2014; Suleimani et al., 2017). Numerous palaeoseismological investigations based on Late Holocene coastal sedimentary records in Japan, Alaska and Chile suggest different patterns of rupture during major, $M7_w - 7.9$, to great, >M8 $_w$, Late Holocene earthquakes compared to those recorded in the 20th and 21st centuries (Briggs et al., 2014; Cisternas et al., 2017; Dura et al., 2015, 2016; Garrett et al., 2015; Kelsey et al., 2015; Nelson et al., 2015; Sawai et al., 2004; Shennan et al., 2014a, 2016; Witter et al., 2014). This raises the question of whether segment boundaries identified for 20th and 21st century major to great earthquakes persist through multiple earthquake cycles, or whether smaller segments with different boundaries rupture and still cause significant hazards.

The eastern segments of the Alaska-Aleutian subduction zone are source areas of significant seismic hazards, generating ≥ M_w 8.0 earthquakes and tsunamis that may propagate across much of the northeast Pacific Ocean. Earthquake source areas include the Prince William Sound and Kodiak segments of the subduction zone, which ruptured together during the M_W 9.2 great Alaska earthquake of 1964, along with the Kenai segment which is currently creeping (Fig. 1). Paleoseismic evidence from coastal sediments currently provide a good record of the recurrence of these great earthquakes especially for the Prince William Sound segment, with widespread evidence of >1 m subsidence or uplift during seven great earthquakes in the last 4000 years (Shennan et al., 2014b) and ten in the last 6000 years (Carver and Plafker, 2008). We know much less about the recurrence of great earthquakes in the Kenai and Kodiak segments and recent investigations from these regions conclude that no earthquake in the last 4000 years had the same spatial pattern of deformation as AD 1964 and that some earthquakes recorded in the Prince William Sound segment may not have crossed the Kenai segment to the Kodiak segment (Kelsey et al., 2015; Shennan et al., 2014a, 2016). In contrast, a single segment rupture occurred in AD 1788, with coseismic land surface deformation across Kodiak Island and a tsunami that is recorded in historical documents (Soloviev, 1990) and in sediment sequences (Shennan et al., 2014a). Coastal paleoseismic evidence reveals another, similar rupture of the Kodiak segment c.500 BP (Carver and Plafker, 2008; Gilpin, 1995; Gilpin et al., 1994; Shennan et al., 2014a). These earthquakes indicate shorter intervals between ruptures of the Kodiak segment than for the Prince William Sound segment. Modelling of tsunami impacts along the coast of

* Corresponding author.
E-mail addresses: ian.shennan@durham.ac.uk (I. Shennan), m.d.brader@durham.ac.uk (M.D. Brader), n.l.m.barlow@leeds.ac.uk (N.L.M. Barlow), f.p.davies@durham.ac.uk (F.P. Davies), christopher.longley@durham.ac.uk (C. Longley), neil.tunstall@durham.ac.uk (N. Tunstall).

https://doi.org/10.1016/j.quascirev.2018.10.028

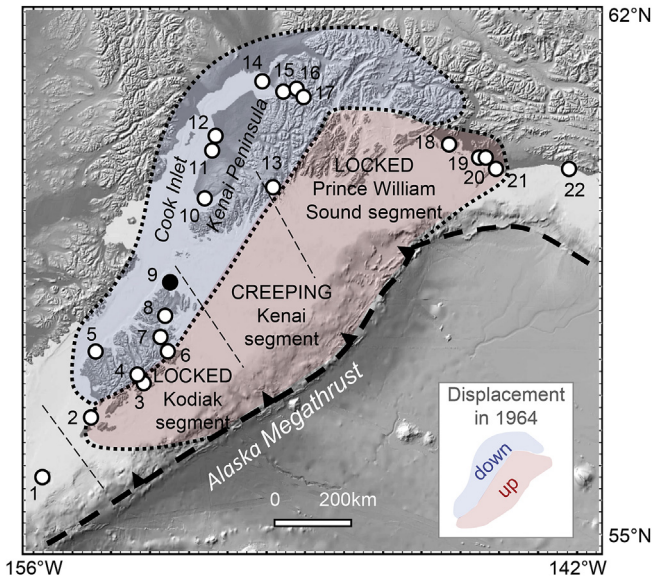

Fig. 1. Tectonic setting and location of paleoseismic sites. Shuyak Island is the solid circle, site 9. Coloured areas show the regions of coseismic uplift and subsidence in AD 1964 (Carver and Plafker, 2008). Plate segments and approximate boundaries are based on GPS measurements of horizontal motion (Freymueller et al., 2008). For detailed information of paleoseismic sites, 1 to 22, see: 1 – Chirikof Island (Nelson et al., 2015); 2 – Sitkinak Island (Briggs et al., 2014); 3 – Sitkalidak Island (Gilpin, 1995); 4 – Three Saints Harbor (Gilpin, 1995); 5 – Karluk Village & Sturgeon Lagoon (Gilpin, 1995; West, 2011); 6 – Middle Bay & Kalsin Bay (Gilpin, 1995; Shennan et al., 2014a, 2016); 7 – Anton Larson Bay (Shennan et al., 2016); 8 – Afognak Island (Carver and Plafker, 2008; Clark, 2008; Gilpin, 1995); 9 – Shuyak Island (this paper and Carver and Plafker, 2008; Gilpin, 1995; McCalpin and Carver, 2009); 10 – Homer (Shennan et al., 2016); 11 – Kasilof River (Shennan et al., 2016); 12 – Kenai River (Hamilton and Shennan, 2005b); 13 – Southeast Kenai Peninsula (Kelsey et al., 2015); 14 – Anchorage (Hamilton et al., 2005); 15 – Hope & Bird Point (Shennan et al., 2016); 16 – Girdwood (Hamilton and Shennan, 2005a; Shennan et al., 2008); 17 – Portage (Shennan et al., 2014b); 18 – Copper River Delta (Carver and Plafker, 2008; Shennan et al., 2014c); 19 – Katalla (Shennan et al., 2014c); 20 – Puffy Slough (Shennan et al., 2014c); 21 – Cape Suckling (Shennan, 2009; Shennan and Hamilton, 2010); 22 – Yakataga (Shennan et al., 2009).

California and Hawaii highlights the hazard that ruptures of single segments of the Alaska subduction zone pose to Pacific coasts, but note the lack of the geological evidence for the ages, recurrence and rupture dimensions of previous earthquakes (Butler, 2012; Kirby et al., 2013; Ryan et al., 2012; SAFFR, 2013).

Shuyak is the northernmost island in the Kodiak archipelago and lies closest to the poorly-defined boundary between the Kodiak and Kenai segments of the Alaska subduction zone (Fig. 1), the eastern part of the Alaska-Aleutian subduction zone that runs across the northern Pacific Ocean, from North America to Asia. Exploratory investigations on Shuyak Island (Gilpin, 1995; Gilpin et al., 1994) describe Late Holocene sediments from five marshes and infer marsh submergence during an earthquake about 500 years ago, with more limited evidence for a younger event and some older events that may be correlated with ruptures of the Prince William Sound segment (Carver and Plafker, 2008). Based on these findings, the present seismic hazard maps for Alaska model characteristic earthquakes for the 1964 rupture zone (Fig. 1), as M_W 9.2 every 650 years, and for the Kodiak segment alone, M_w 8.8 every 650 years (Mueller et al., 2015; Wesson et al., 2007, 2008). Tsunami hazard assessments embrace a wider range of scenarios for different modes of rupture, including single segment ruptures and variations in the depth of rupture (Suleimani et al., 2017). These illustrate the spatial variability of surface deformation across the Kodiak archipelago during earthquakes with different distributions of slip along the subducting plate interface, or megathrust (Fig. 2).

Shuyak Island therefore offers the best opportunity to record coseismic deformation at the northern extent of the Kodiak segment, and in combination with other sites potentially constrain rupture dimensions of previous earthquakes in addition to their ages and recurrence. In this paper we aim to (1) establish the spatial extent of evidence for Late Holocene earthquakes in stratigraphic sequences from Shuyak Island, (2) determine the extent of deformation for each earthquake, and (3) evaluate the persistence, or non-persistence of rupture boundaries between the Kodiak and the Kenai and Prince William Sound segments.

2. Field locations

The outer coasts of Shuyak Island are exposed to high energy waves generated by storm systems crossing the Shelikof Straight or the northern Pacific. In the northwest part of the island there are numerous sheltered bays and channels (Fig. 3). Small tidal marshes contain sediment sequences that record coseismic subsidence in AD 1964 and evidence of earlier earthquakes (Carver and Plafker, 2008; Gilpin, 1995; Gilpin et al., 1994; McCalpin and Carver, 2009). In contrast to the sediment-rich depositional environments of most of the sites from the Prince William Sound and Kenai segment, the marshes on Shuyak Island have small terrestrial catchments of low relief and are sediment poor (Fig. 3).

Reoccupation of a temporary tidal benchmark in Carry Inlet (Fig. 3B) in 1965 (Plafker, 1969) and 1993 (Gilpin, 1995) estimate 1.05 m coseismic subsidence in 1964 and 0.45 m post-seismic uplift in the following 29 years, each with an uncertainty in the order of ±0.1 m. Predicted Mean Higher-High Water (MHWW) is ~1.24 m above Mean Sea Level (Supplementary Information and NOAA, 2016).

3. Methods

We sampled four sites, Deer Marsh, Skiff Passage Marsh, Bear Trail Marsh and South Carry Inlet (Fig. 3), using cleaned outcrops and hand driven cores to determine the lateral continuity of sediment layers prior to selecting which samples to return to the laboratory for analysis.

3.1. Diatom analyses

At Bear Trail Marsh we collected 30 samples for modern diatom assemblages from the sediment surface, from the low water mark, across the tidal flat and tidal marsh to above the limit of highest tides, measuring the elevation of each sample with respect to high tide level. We used a stratified sampling design to give an approximately evenly-spaced distribution in terms of elevation with a random pattern for spatial location. We incorporate the modern surface samples into our previous Alaska training set (Shennan et al., 2016) to produce new transfer function models to reconstruct marsh surface elevation and use the new models to reconstruct surface elevation changes through the fossil sequences.

In previous transfer function-based analyses we used a regional-scale modern training set collected from a wide range of marshes across ~1000 km of south central Alaska in order to seek the best fit between fossil and modern diatom assemblages (Watcham et al., 2013). This approach applied three models, constrained by the lithology of the Holocene sediment sequence; one for peat sediment, a second for organic silt units and silt units with visible plant rootlets, and a third for silt units with no rootlets. This approach is less applicable to sediments sequences, such as those on Shuyak, where there is less clear distinction between layers of different organic content and the lateral continuity of deposits is difficult to establish, with non-continuous silt and sand lenses evident at most

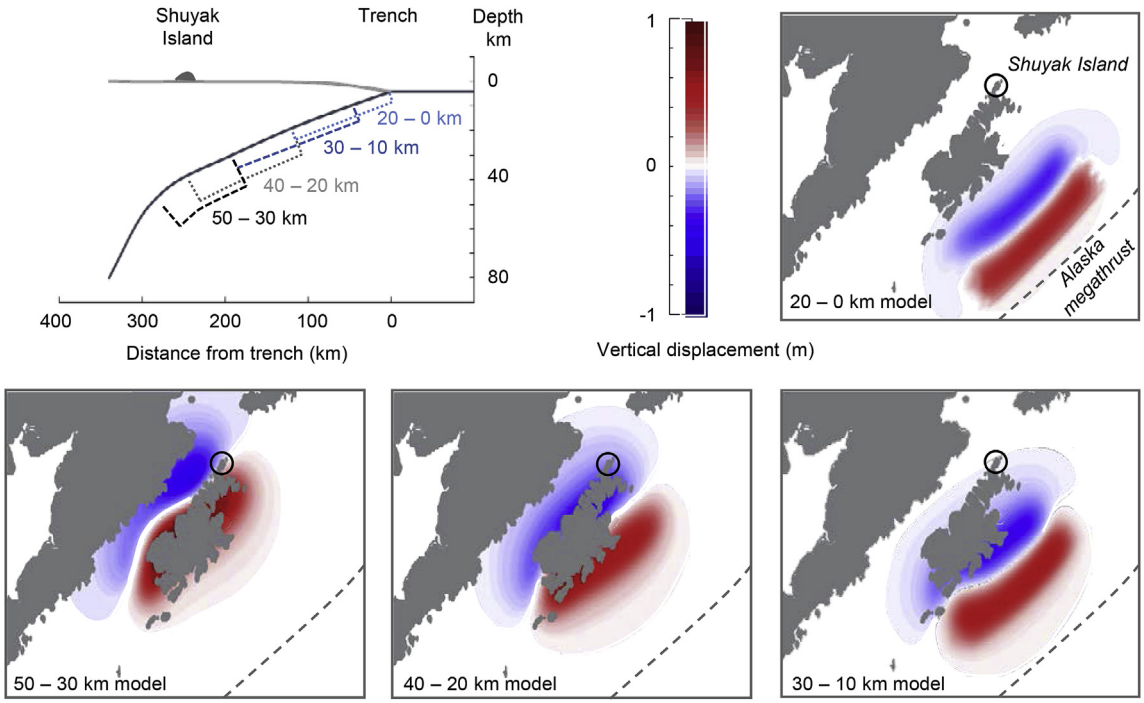

Fig. 2. Computed vertical ground-surface deformation for four hypothetical M_w 8.0 ruptures in the area of Kodiak Island (Suleimani et al., 2017). Map elements extracted and modified from multiple plots in Suleimani et al. (2017). The slip location varies in the downdip direction of the interface between the Pacific plate which is subducting beneath the North American plate (Top left; e.g. "40–20 km" model has all slip occurring on the plate interface between 40 and 20 km depth).

sites. Therefore, for our estimates of paleo-marsh surface elevations we employ two different transfer function models, using the C2 package (Juggins, 2014).

The first uses the modern samples from three sites: Middle Bay, on Kodiak Island; Beluga Slough at Homer; and our new data from Bear Trail Marsh, and follows the weighted average partial least squares (WA-PLS) method of our previous studies. These three sites are more likely to reflect past conditions on Shuyak Island better than modern samples from marshes in Cook Inlet where water salinity decreases with distance from the open ocean. The three sites produce a modern data set of 130 samples and a squared correlation between bootstrap predicted and observed values (r^2) of 0.77. As with our previous studies, we assess goodness of fit between each fossil sample and the modern dataset with a dissimilarity coefficient, using the 20th percentile of the dissimilarity values for the modern samples as the cut-off between 'close' and 'poor' modern analogues for fossil samples, and the 5th percentile as the threshold for defining 'good' modern analogues (Hamilton and Shennan, 2005a). All samples from the outcrops and cores give good or close modern analogues using the Shuyak-Kodiak- Homer subset of 130 modern samples. For reconstruction of the elevation at which the fossil sediment accumulated, termed paleomarsh surface elevation (PMSE), we present sample-specific 95.4% (2σ) error terms.

Our second transfer function model uses a more recently developed method, a locally weighted weighted-averaging (LW-WA) transfer function (Kemp and Telford, 2015). This method aims to strike the balance between a small, local dataset to reconstruct sea level and a large dataset encompassing a wide range of modern analogues available from across the whole of south-central Alaska. This method creates a modern training set for each fossil sample based on a subset of 30 samples, from the total 326 across the region, with the smallest dissimilarity coefficients, and uses these 30 in a weighted average transfer function model. This gives a squared correlation between bootstrap predicted and observed values (r^2) of 0.81 and a smaller root mean square error of prediction, ~70% of our WA-PLS model.

In the following sections, we show a summary of the diatom data and changes in paleo-marsh elevation derived from the transfer function models. Supplementary files contain the full diatom data. In order to summarise the diatom data, we classify each species according to their mean elevation (defined by the bootstrap species coefficient from the WA-PLS transfer function model) in the modern data set: below mean sea level (MSL); mean sea level to mean higher high water (MHHW); above mean higher high water; or unclassified. This classification scheme provides a visual aid to summarise the assemblage changes but does not take into account the elevation range of each species, only the mean. In contrast, the transfer function model reconstructions do account for these ranges.

3.2. Geochemical analyses

We used a Geotek XRF to provide magnetic susceptibility, concentrations of 21 elements at 2 mm intervals, and high resolution photographs for each core/box sample from outcrops. We use the high-resolution images to measure the sharpness of sediment boundaries in addition to those recorded in the field. From the elemental analyses, we see no clear relationship with changes across sediment boundaries and in a similar fashion to Nelson et al. (2015) do not speculate on how they may reflect one or more different processes. We provide the data in a supplementary file.

3.3. Radiocarbon data and age modelling

We submitted 43 samples for AMS radiocarbon dating, picking herbaceous macrofossils from the sediment (Table 1). We derive an age model for each site with Oxcal 4.3 (Bronk Ramsey, 2001, 2008),

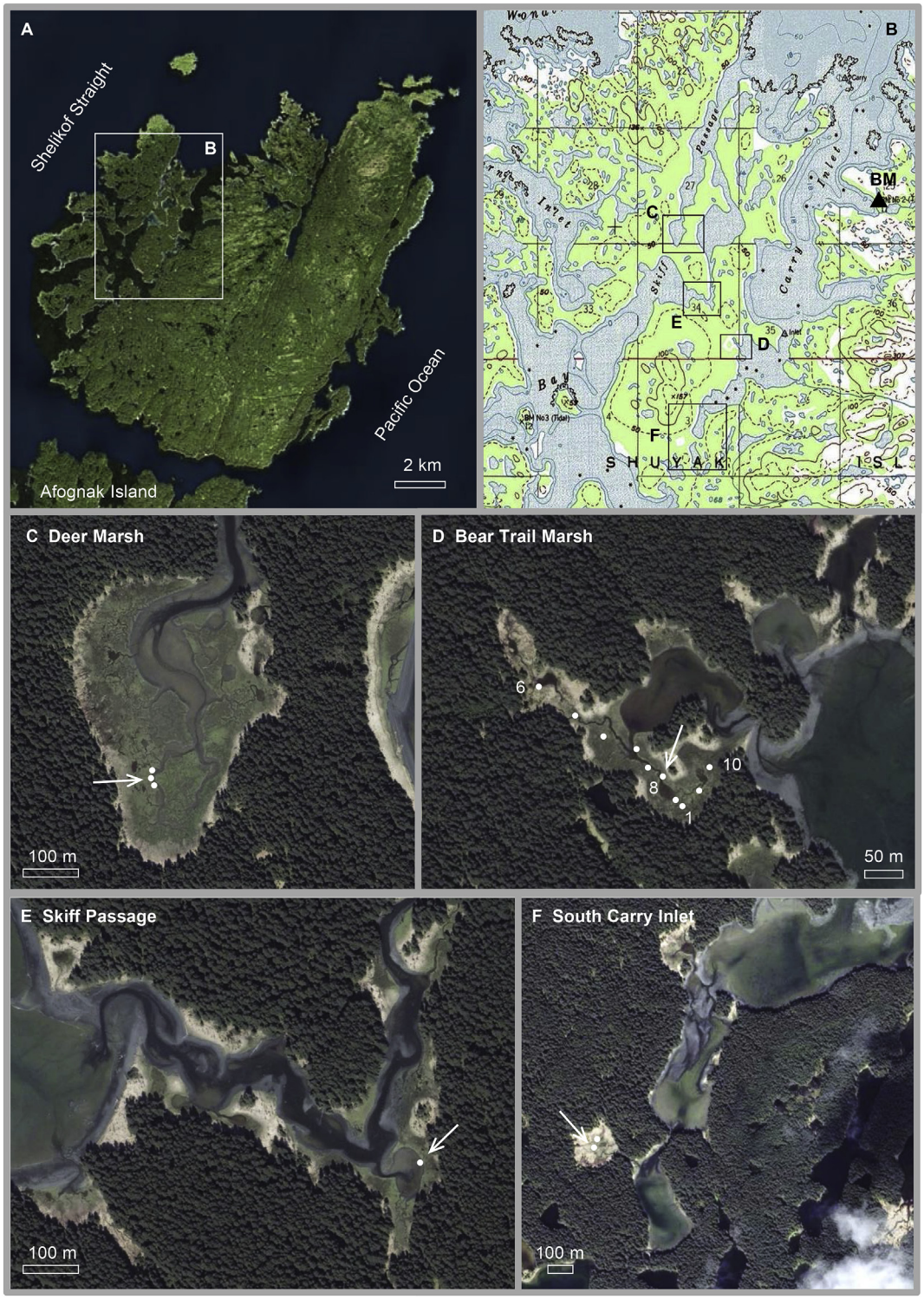

Fig. 3. (A) Shuyak Island and north coast of Afognak Island. (B) USGS Topographic map, 1987 edition, based on 1952 survey, with 1 mile, 1.61 km, grid lines. BM = temporary tidal bench mark used to estimate coseismic subsidence (Plafker, 1969; Plafker and Kachadoorian, 1966) and post-seismic uplift (Gilpin, 1995). (C to F) Field sites with locations of recorded outcrops and cores, arrow indicates samples used for laboratory analyses. Aerial images, www.bing.com accessed May 2016, note differences with pre-earthquake coastline (B, topographic map) at Bear Trail Marsh (D) and South Carry Inlet (F). At Bear Trail Marsh, the white circular area in B is now the tidal marsh, with the core locations, and tidal flat (D). At South Carry Inlet (F) the site we cored is the white circular area in B, and it drains into a tidal lagoon which is a lake not connected to the sea in B.

using the P_Sequence model, which allows for a variable sediment rates, building in a hiatus at each sharp boundary between sediment layers, and constrain the model at the base of the distinct Katmai tephra, AD 1912 (Hildreth, 1983). We set the model parameters to generate age estimates at 1 mm intervals and therefore modelled ages for each diatom sample.

Table 1
Radiocarbon results. All are AMS samples from herbaceous plant material (leaves, stems and seeds), with ages calibrated from CALIB v7 (Stuiver et al., 2017).

Location	Laboratory code	Stratigraphic position (cm)	$\delta^{13}C_{VPDB}$‰ ± 0.1	^{14}C Enrichment (% modern)	+/− 1σ (% modern)	Conventional Radiocarbon Age (yrs BP)	+/− 1σ (^{14}C yrs BP)	Calibrated age BP median probability	95% age range BP	
Deer Marsh Outcrop 2										
	OS-132048	41	−26.60	0.9779	0.0020	180	15	183	284	1
	SUERC-75712	45	−24.07	97.12	0.42	235	35	279	426	1
	SUERC-75713	49	−24.52	97.99	0.45	163	37	173	288	1
	SUERC-75714	53	−24.78	97.31	0.42	219	35	188	420	1
	SUERC-75715	57	−25.01	97.72	0.43	185	35	180	301	1
	SUERC-75716	61	−24.71	97.79	0.43	179	35	179	300	1
	SUERC-75717	65	−25.69	97.86	0.45	174	37	177	297	1
	OS-132049	68	−24.98	0.9738	0.0019	215	15	166	300	1
	SUERC-75721	69	−27.04	97.72	0.45	186	37	179	303	1
	SUERC-75722	73	−26.86	98.00	0.43	162	35	174	287	1
	OS-132050	78	−26.29	0.9663	0.0019	275	15	308	423	292
	OS-132051	81	−26.53	0.9666	0.0019	275	15	308	423	292
	OS-132052	83	−25.04	0.9609	0.0019	320	15	387	454	308
	OS-132053	87.5	−25.12	0.9607	0.0019	320	15	387	454	308
	SUERC-75724	92	−26.16	95.62	0.42	360	35	410	500	315
	SUERC-75725	96	−26.93	94.76	0.44	433	37	496	535	332
	SUERC-75726	98.5	−27.04	95.07	0.41	406	35	474	519	320
	SUERC-75727	101	−26.78	94.74	0.43	434	37	497	536	332
	SUERC-75732	104	−26.67	93.42	0.41	547	35	555	641	513
	OS-132054	106	−25.80	0.9255	0.0018	620	15	598	654	555
Bear Trail Marsh Outcrop 8										
	SUERC-75733	33	−26.26	101.79	0.44	F Modern 1.0179				
	SUERC-75734	36.5	−26.23	98.88	0.45	91	37	112	269	13
	OS-132165	38	−26.33	0.9766	0.0019	190	15	175	287	1
	SUERC-75735	41	−27.54	98.11	0.45	153	37	161	284	1
	SUERC-75736	44.5	−26.60	97.99	0.45	163	37	173	288	1
	OS-132164	46	−25.64	0.9799	0.0020	165	15	190	282	2
	SUERC-75737	49	−26.95	98.76	0.43	100	35	114	269	12
	SUERC-75741	53	−26.40	98.45	0.45	126	37	129	276	8
	SUERC-75742	57.5	−26.82	97.30	0.42	220	35	189	420	1
	SUERC-75743	61	−27.28	96.23	0.44	309	37	387	472	298
	OS-132163	65	−26.49	0.9334	0.0019	555	15	551	628	530
	OS-132162	67	−26.67	0.9386	0.0019	510	15	529	541	515
	SUERC-75744	68	−27.50	89.68	0.39	875	35	784	909	705
	SUERC-75745	72	−27.66	90.03	0.41	843	37	752	900	684
	OS-132161	77	−26.43	0.7923	0.0016	1870	15	1823	1870	1737
Skiff Passage Marsh Outcrop										
	OS-132062	23	−27.29	1.0121	0.0020	F Modern 1.0121				
	OS-132061	75	−26.27	0.9788	0.0020	170	15	188	283	1
	Beta-485799	87	−26.00	0.9669	0.0036	270	30	319	435	1
	OS-132060	103	−26.19	0.9074	0.0018	780	15	698	727	679
	OS-132059	110	−26.74	0.9094	0.0021	765	20	689	726	672
	OS-132058	119	−27.68	0.9144	0.0022	720	20	673	686	659
	OS-132057	120	−27.37	0.8727	0.0025	1090	25	996	1057	938
	OS-132056	130	−27.57	0.8539	0.0017	1270	15	1230	1267	1181
South Carry Inlet Marsh borehole 2										
	OS-132055	456	−25.91	0.2753	0.0016	10,350	45	12211	12396	12016

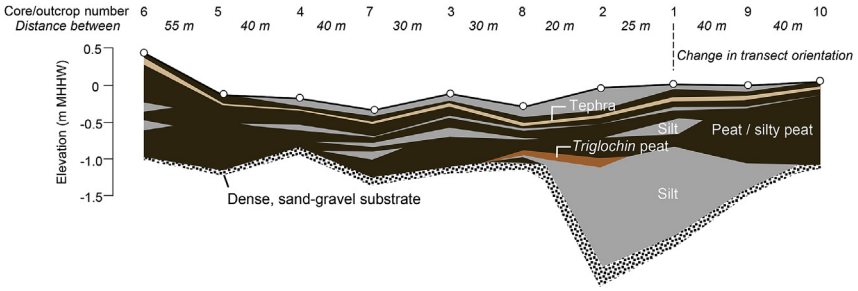

Fig. 4. Stratigraphy across Bear Trail Marsh from outcrops (locations 7 and 8) and cores.

4. Results

4.1. Bear Trail Marsh

The stratigraphic transect, from eight cores and two cleaned outcrops (Figs. 3D and 4), enables us to trace stratigraphic contacts across the site. At all locations except for site 6, we can trace an abrupt boundary between peat overlain by organic silt with rootlets between 0.05 and 0.30 m below the ground surface. We interpret this as rapid submergence of the marsh during the 1964 earthquake. The pre-1964 topographic map shows this part of the marsh as unforested but above the high tide line (Fig. 3B) and the contrast with the aerial images (Fig. 3C–F) shows the net effect of marsh changes since submergence in 1964.

The next traceable horizon down section is a light coloured silt, sometimes slightly orange or pink, which we see in all cores and trench sections (Fig. 4), at depths from ~0.1 to 0.5 m. This is the Katmai tephra of AD 1912 (Hildreth, 1983). The Katmai tephra is pervasive across the landscape and a clear region-wide stratigraphic marker on Shuyak Island and the rest of the Kodiak archipelago.

In the peat-dominated sequence, from beneath the Katmai tephra to a sand and gravel-rich basal horizon, we recorded a number of clastic-rich layers but some are difficult to correlate across the marsh. Across most of the transect, locations 4 to 9, ~0.1–0.2 m below the base of the Katmai tephra, there is a thin clastic unit with a sharp contact to the underlying peat. Between 0.5 and 1 m below surface there are some thicker clastic units, varying from silt to organic silt, which are difficult to correlate between cores. In outcrops, locations 7 and 8 (Figs. 4 and 5), we see additional clastic layers, including sand and gravel, some pinch out, others extend across the cleaned section. Some of the boundaries between these layers are diffuse, others are sharp.

The diatom-based reconstructions (Fig. 6) indicate marsh surface elevation varying very little, between −0.7 and 0.0 m MHHW, with changes across sediment boundaries mostly no greater than changes between adjacent samples within the silt peat layers. These reconstructions compare favourably with the similarity between the sediment lithology (Fig. 5) and the elevation ranges of modern marsh vegetation and sediment zones (Fig. 7). The reconstructions reflect a balance between vegetated marsh and mud, mainly silt but other finer and coarser fractions, within a similar elevation range.

Three minerogenic-dominated layers in outcrop 8 (Fig. 5), each with a sharp contact to the peat below, are similar to stratigraphic changes considered as evidence of metre-scale subsidence (Gilpin,

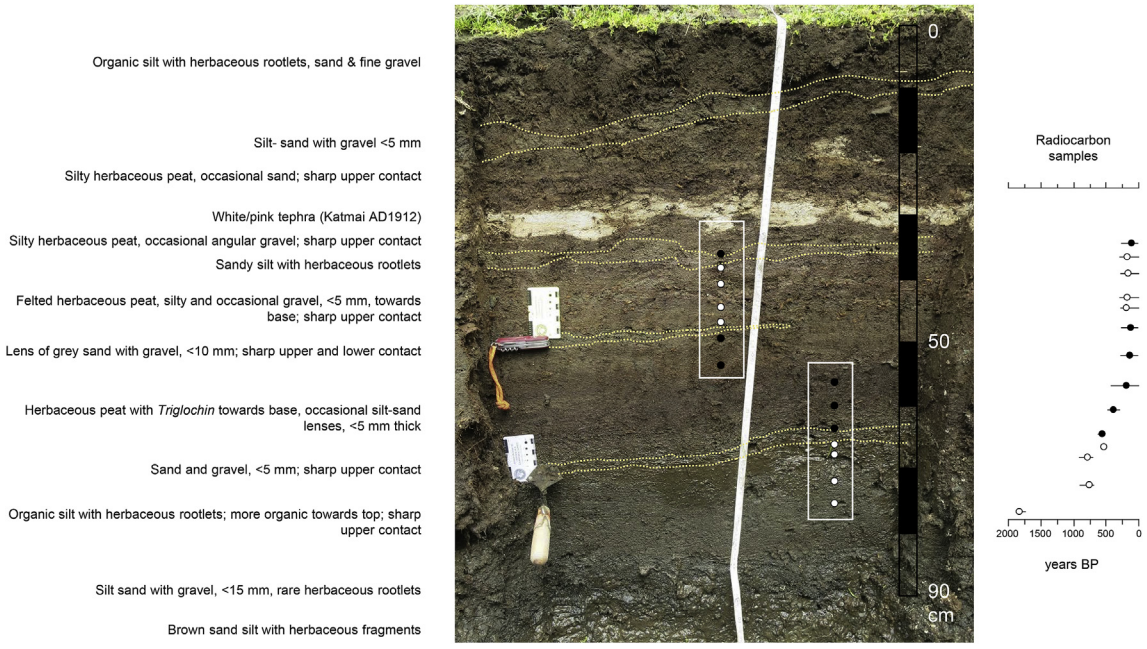

Fig. 5. Bear Trail Marsh outcrop, location 8. White rectangles indicate the position of the 0.25 m box samples taken for laboratory analyses. Radiocarbon samples, details in Table 1, shaded differently to aid correlation between the boxes. Scale inserted on the right-hand side with no correction for the angle of the camera – depths in the text refer to those at the position of the box samples and may differ slightly.

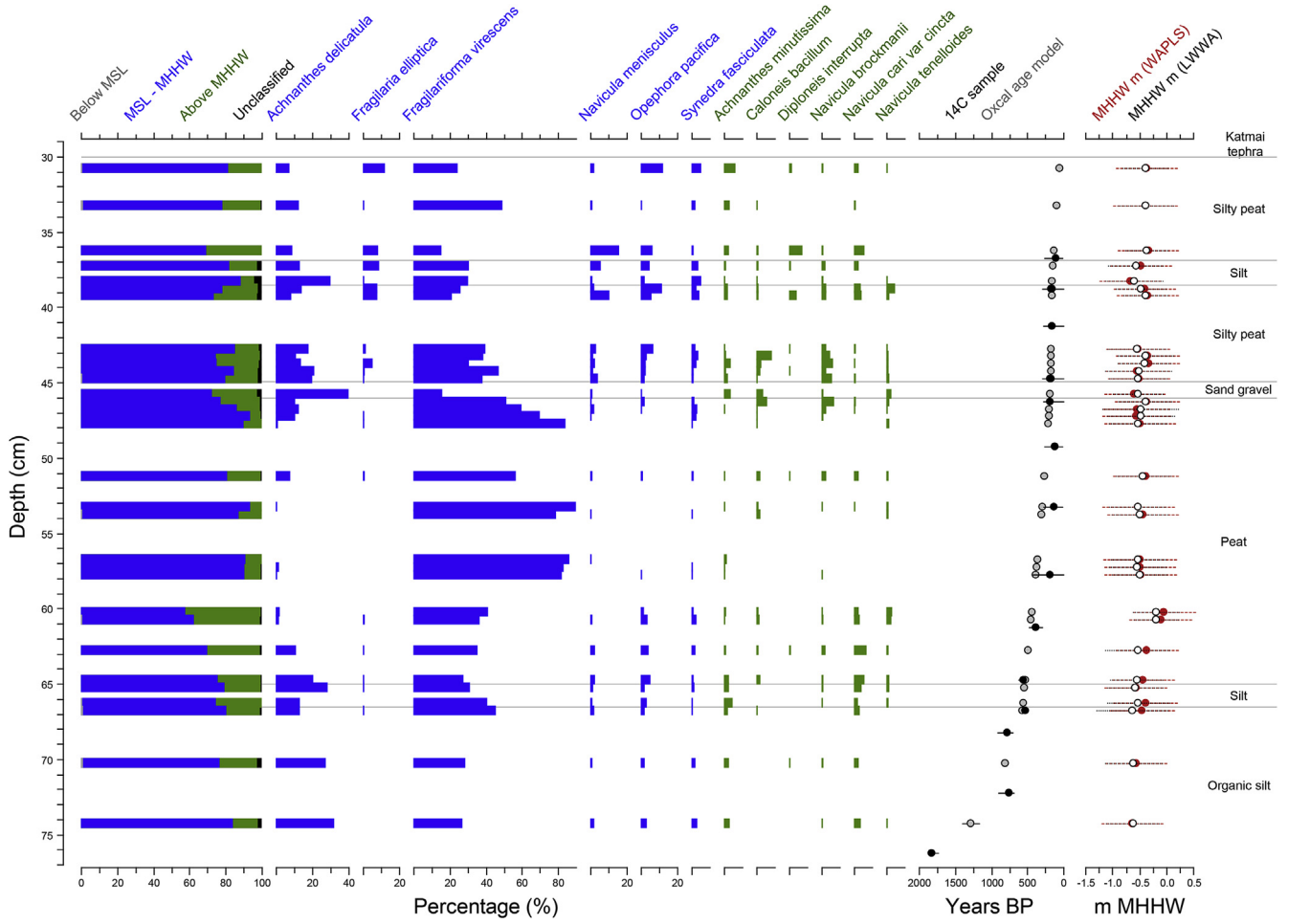

Fig. 6. Bear Trail Marsh outcrop between the basal gravel and Katmai tephra (AD 1912). Diatom summary classes based on species optimal elevations in the modern dataset, species shown are those with frequencies >10%. Age model shows each radiocarbon sample (black) and the Oxcal modelled age (grey) for each diatom sample. Right-hand graph shows changes in paleo-marsh surface elevation, with 95% confidence limits, estimated by two transfer function models (see text).

1995; McCalpin and Carver, 2009).

The diatoms in the lowermost minerogenic layer, 65–66.5 cm, suggest no elevation change across the lower contact or across the contact to peat above. Significantly, the peat above the sand is rich in *Triglochin* macrofossils whereas the peat below is not. Similar evidence was previously interpreted as suggesting ~1 m coseismic subsidence. Our diatom results do not support such an interpretation. *Triglochin* occurs in the modern marsh within approximately the same elevation range as the transition from <10% vegetation cover to 100% cover, ~-0.6 to +0.2 m MHHW (Fig. 7). Within this range there is a spatial mosaic of variable vegetation cover and abundances of numerous plant species. Changes across the boundary between sediment layers in an outcrop or core may reflect vegetation succession and sediment dynamics within this transition zone, with little or no elevation change with respect to contemporaneous tide levels. Changes in the abundance of one species need not reflect elevation change in the order of 1 m. We observe a temporary input of clastic sediment, 65–66.5 cm, followed by a change in marsh vegetation but no major change in elevation (Fig. 6). In contrast, at 60 to 58 cm the peat changes colour (Fig. 5) and has fewer *Triglochin* above this transition. The diatom reconstructions indicate submergence, >0.30 m (Fig. 6).

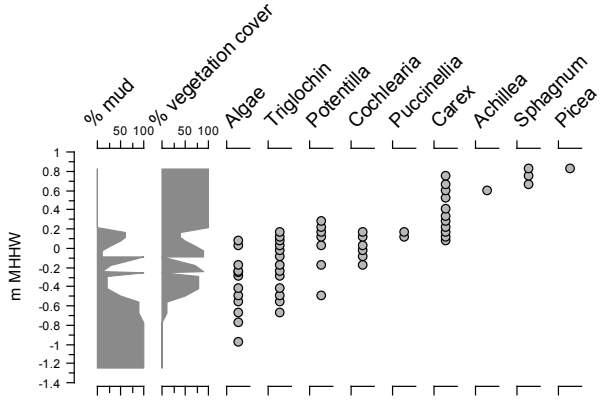

Fig. 7. Bear Trail Marsh surface sediment and vegetation cover recorded at the 30 samples taken for the modern diatom assemblages. Named genera shown when recorded in the field as abundant.

For the middle minerogenic unit, a lens of sand with gravel at 45–46 cm which does not extend across the whole of the outcrop, there is a temporary peak of one diatom species but we see no change in elevation from the silt peat below to the silt peat above.

The upper minerogenic layer, 36.5–38.5 cm, shows a drop in elevation across the sharp lower contact and a gradual recovery into the overlying silt-peat. The estimates change in elevation across the sharp lower contact is model-dependent, −0.13 m (LWWA) and −0.27 m (WAPLS). Both of these are smaller than the 95% uncertainty terms (~0.5–0.6 m).

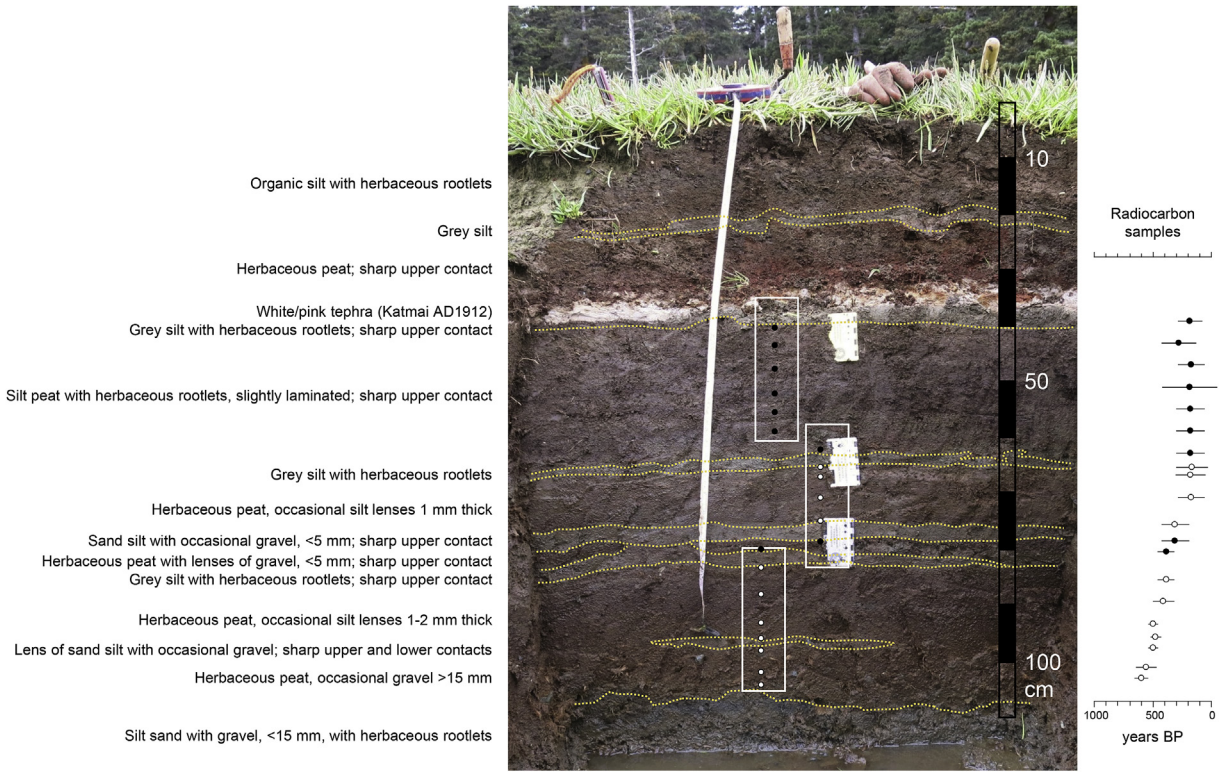

Fig. 8. Dear Marsh outcrop. White rectangles indicate the position of the 0.25 m box samples taken for laboratory analyses. Radiocarbon samples, details in Table 1, shaded differently to aid correlation between the boxes. Scale inserted on the right-hand side with no correction for the angle of the camera – depths in the text refer to those at the position of the box samples and may differ slightly.

4.2. Deer Marsh

Deer Marsh occupies a sheltered tidal inlet off the northern arm of Skiff Passage (Fig. 3). We cleaned three outcrops, 10 and 15 m apart, along a tidal channel, taking box samples from the middle outcrop for laboratory analyses.

The Katmai tephra is distinct in all three outcrops along with a grey silt immediately below, overlying silt peat with a sharp upper contact. Midway between the Katmai tephra and the surface (Fig. 8), a change from brown herbaceous peat, with a sharp upper contact, to grey silt suggests rapid submergence, which we interpret as AD 1964. Brown organic silt with herbaceous rootlets in the uppermost 15–20 cm indicate marsh colonisation during the post-seismic period. It is more difficult to correlate other layers across the three outcrops (Shennan et al., 2017).

The section below the Katmai tephra indicates ~70 cm sediment accumulation between c.600 BP and AD 1912. The elevation reconstructions show little change during this period, indicating sediment accumulation keeping pace with relative sea-level rise. Four changes in sediment type indicate possible episodes of more rapid change.

The sand-silt lens at 99–101 cm does not extend across the whole of the outcrop (Fig. 9) and there is no similar layer in the other two outcrops, but it has different diatom assemblages to the peat above and below, and the assemblages indicate a lower elevation. The limited extent of this layer would suggest a local effect, such as sediment reworking, rather than coseismic subsidence.

In mid-section, 78–88 cm, we see a complex stratigraphy, with one silt layer which extends across the whole of the outcrop, but it is split across much of the outcrop by an intervening peat which itself contains discrete sand/gravel lenses. All of the upper and lower contacts of these silt, peat and sand/gravel units are sharp (Fig. 8). Similar, though discontinuous silt units occur at comparable stratigraphic positions in the other two outcrops at Deer Marsh (Shennan et al., 2017). Our box samples cross the most complex section, with two silt layers and the intervening peat with a sand/gravel lens. The diatom assemblages and elevation estimates indicate abrupt submergence, in the order of 0.2–0.3 m at the base of the complex section, the peat-silt contact at 88 cm. The radiocarbon ages indicate no clear hiatus between the top of the peat at 88 cm and the base of the peat at 78 cm, above this complex section. We conclude that the thin peat with sand/gravel lens that splits the silt layer into two in the sampled section likely indicates some reworking during the period of silt deposition.

In contrast to these two silt layers, the silt at 65.5–67.5 cm has a sharp lower contact but a transitional upper contact, suggesting rapid submergence and gradual recovery, although the diatom-based reconstructions suggest no elevation change across the sharp lower contact.

The laminated silt-peat unit ends 4 cm below the Katmai tephra, with a sharp upper contact to grey silt. This silt also occurs across one other outcrop, while in the third it is only 1 cm thick and pinches out within the peat unit, 1 cm below the tephra. Changes in diatom assemblages indicate marsh submergence ~0.15 m, but only in the WAPLS transfer function model.

4.3. Skiff Passage Marsh

At Skiff Passage, we cleaned and sampled a marsh outcrop at the edge of a small lagoon between the main tidal channel and the spruce forest (Fig. 3). This is the same lagoon described by Gilpin (1995) and used subsequently as an idealised stratigraphic model to record two pre-AD 1964 earthquakes (McCalpin and Carver,

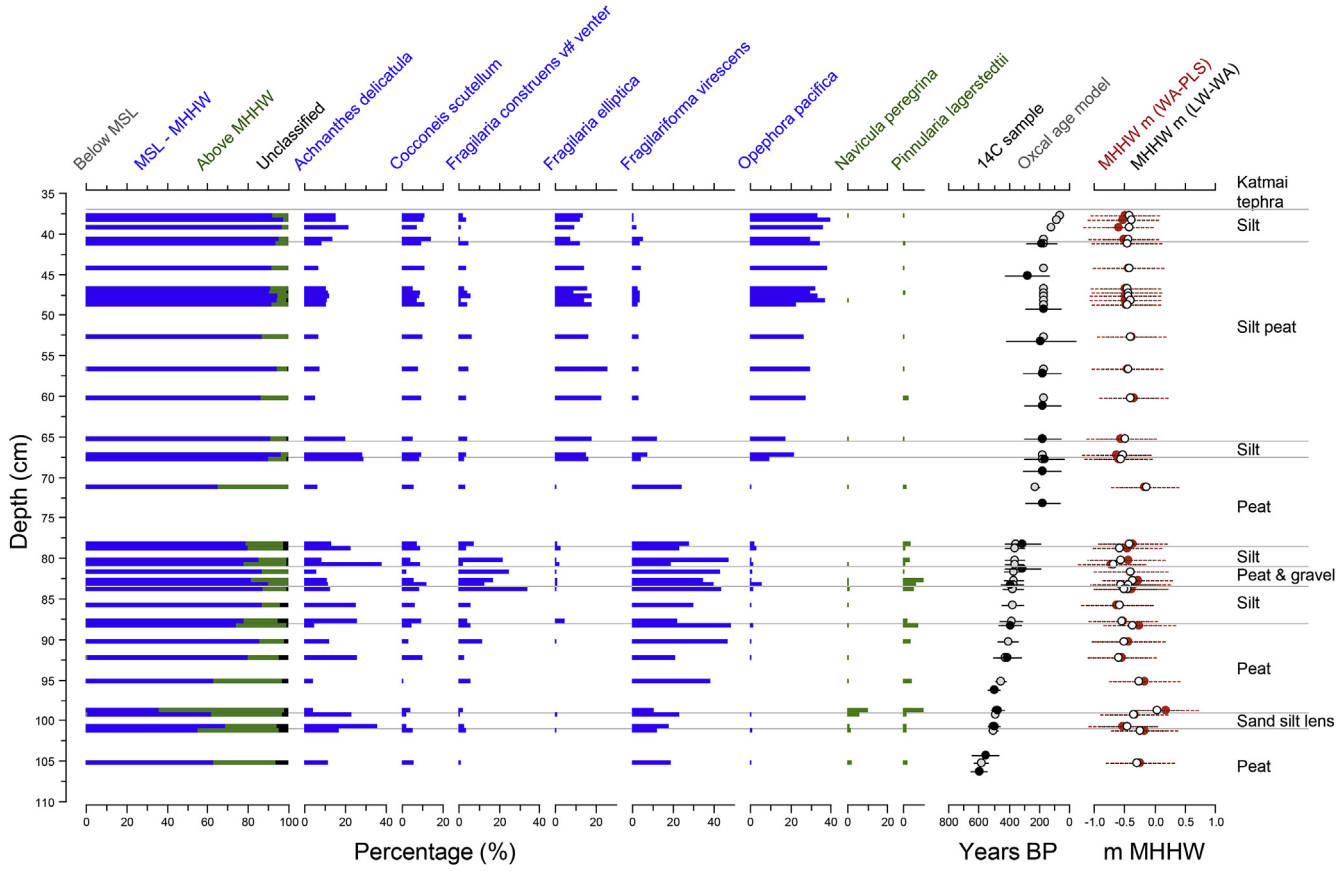

Fig. 9. Deer Marsh outcrop between the basal sand-silt-gravel and Katmai tephra (AD 1912). Diatom summary classes based on species optimal elevations in the modern dataset, species shown are those with frequencies >10%. Age model shows each radiocarbon sample (black) and the Oxcal modelled age (grey) for each diatom sample. Right-hand graph shows changes in paleo-marsh surface elevation, with 95% confidence limits, estimated by two transfer function models (see text).

2009). These studies noted the discontinuous nature of some of the minerogenic layers but also highlighted that they sometimes coincide with sharp boundaries between peat without *Triglochin* macrofossils and *Triglochin*-rich peat, which they interpreted as evidence of late Holocene earthquakes. We record five similar changes in lithology (Fig. 10).

The radiocarbon ages indicate two hiatuses, the first at 120 cm, where *Triglochin*-rich peat overlies herbaceous peat, with a sharp contact, and a second across the sand-gravel bed of variable thickness which extends across the whole outcrop ~90–100 cm below the surface.

Diatoms across the change in peat type at 120 cm (Fig. 11), with a sharp contact and hiatus of a few hundred years indicated by the radiocarbon ages, show minor, net submergence in the WAPLS

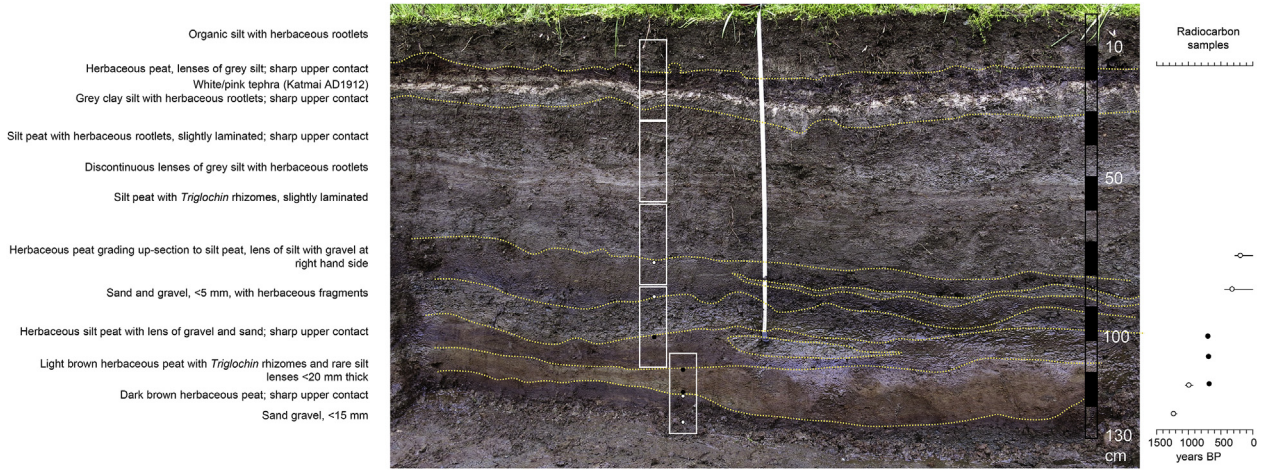

Fig. 10. Skiff Passage Marsh outcrop. White rectangles indicate the position of the 0.25 m box samples taken for laboratory analyses. Radiocarbon samples, details in Table 1, shaded differently to aid correlation between the boxes. Scale inserted on the right-hand side with no correction for the angle of the camera – depths in the text refer to those at the position of the box samples and may differ slightly.

model. Radiocarbon ages within the overlying peat layers indicate rapid accumulation through the peat layer prior to the sharp boundary from herbaceous peat to silt-sand-gravel at 103 cm and the second hiatus. We have no indication of when the silt-sand-gravel was deposited during this hiatus. The diatoms do not indicate submergence, rather the diatoms in the peat above, at 89 cm, compared to the peat below, 104 cm, indicate net emergence in the order of 0.6 m across the hiatus.

At 75 cm there is another change from herbaceous peat to *Triglochin*-rich peat, but, in contrast to the boundary at 120 cm the boundary is gradual and there is no consistent change in the elevation reconstructions to support submergence.

A little below the Katmai tephra, silt-clay abruptly overlies silty herbaceous peat. Diatom assemblages indicate minor submergence across the sharp contact at 23.5 cm. Above the Katmai tephra, we interpret the sharp contact from peat to organic-rich silt at 14 cm as the record of the AD 1964 earthquake. The diatom assemblages indicate ~0.3 m submergence.

4.4. South Carry Inlet Marsh

Comparison of the pre-1964 USGS topographic maps with recent aerial imagery illustrates the effect of coseismic subsidence in AD 1964 (Fig. 3). It transformed a freshwater lake at the southern end of Carry Inlet into a tidal inlet. To the northwest of the new inlet, which we refer to as South Carry Inlet, there is now an intertidal marsh connected to the inlet (Fig. 3F) through a narrow channel across a rock sill (Fig. 12). The pre-1964 maps show this as an open area within the forest (Fig. 3B). Small patches of dead trees, or ghost forest, suggest rapid submergence of a freshwater environment to intertidal marsh.

Two hand-driven cores reveal almost 5 m of sediment before gravel prevented further sampling. Both cores record blue-grey clay-silt above the impenetrable gravel. This grades upwards to olive-green organic (limnic) mud. Within this mud, there are occasional 0.5–5 cm thick minerogenic layers, which we interpret as a series of tephras. Around 50–60 cm below the surface, the limnic mud grades to a peat rich in herbaceous and *Sphagnum* roots. We interpret a 4 cm thick white tephra ~20 cm below the surface as the AD 1912 Katmai tephra. In the lowest areas, closest to the connection to South Carry Inlet, the surface ~10 cm is silt peat, reflecting intertidal sedimentation since AD 1964.

Diatom analyses in the sediments below the Katmai tephra reveal exclusively freshwater environments and support our interpretation of limnic mud accumulation. The basal blue-grey clay silt also has freshwater diatoms, as do the minerogenic layers within the limnic mud. The root-rich peat below the Katmai tephra similarly has only freshwater diatoms.

The sediment stratigraphy, coastal morphology and diatom data suggest that following deglaciation South Carry Inlet Marsh was a freshwater lake. As climate warmed, biological productivity increased and organic limnic mud accumulated. The radiocarbon age from the base of the mud, >12 ka BP (Table 1), is a minimum for the age of deglaciation and the onset of biological productivity within the lake. At this point, relative sea level was below the elevation of the outflow of the lake. This contrasts with the raised shorelines and terraces of similar age seen on the Kenai Peninsula (Reger et al., 2007). As limnic mud accumulated, the lake became shallower and eventually colonised by freshwater herbaceous and *Sphagnum* communities, forming peat. There is no evidence of any marine incursions into the site prior to AD 1964. This provides a valuable constraint on reconstructing the net effects of elevation changes through proposed multiple earthquake cycles.

5. Discussion

5.1. The evidence for multiple Late Holocene earthquakes on Shuyak Island

Our first research question addresses whether we can establish the spatial extent of evidence for multiple Late Holocene earthquakes in stratigraphic sequences from Shuyak Island. Initially we

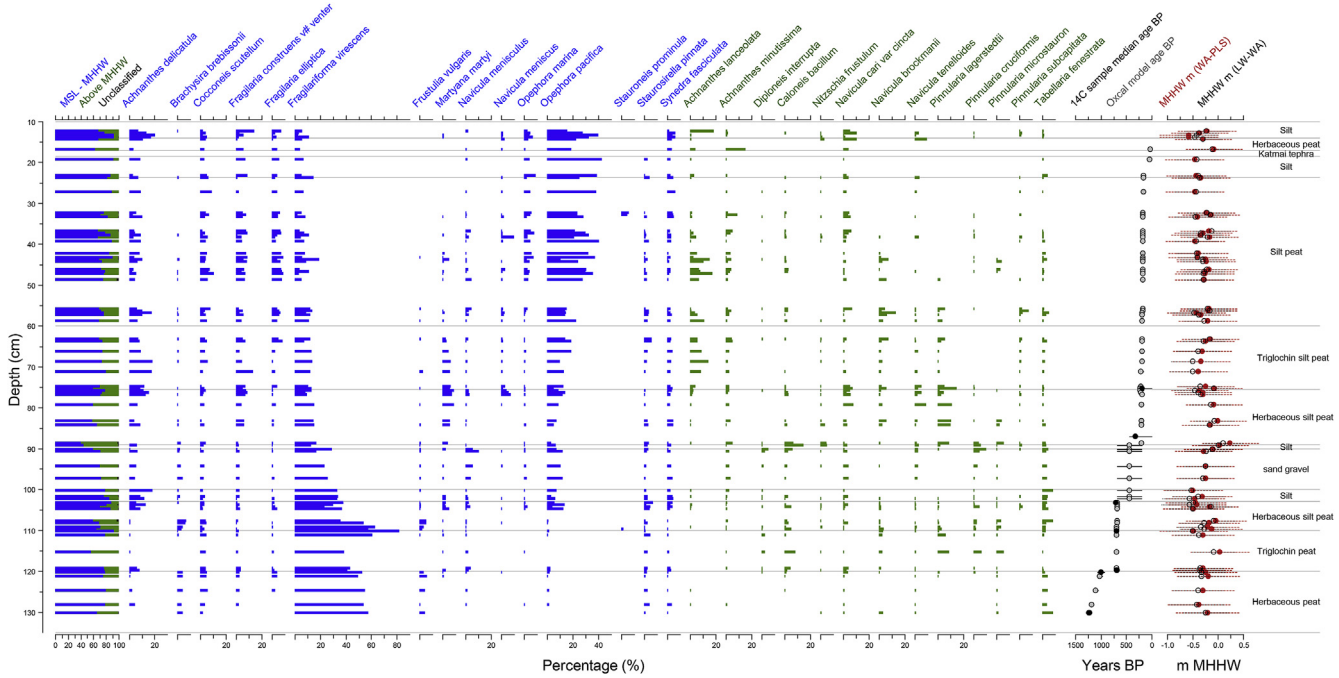

Fig. 11. Skip Passage Marsh outcrop. Diatom summary classes based on species optimal elevations in the modern dataset, species shown are those with frequencies >10%. Age model shows each radiocarbon sample (black) and the Oxcal modelled age (grey) for each diatom sample. Right-hand graph shows changes in paleo-marsh surface elevation, with 95% confidence limits, estimated by two transfer function models (see text).

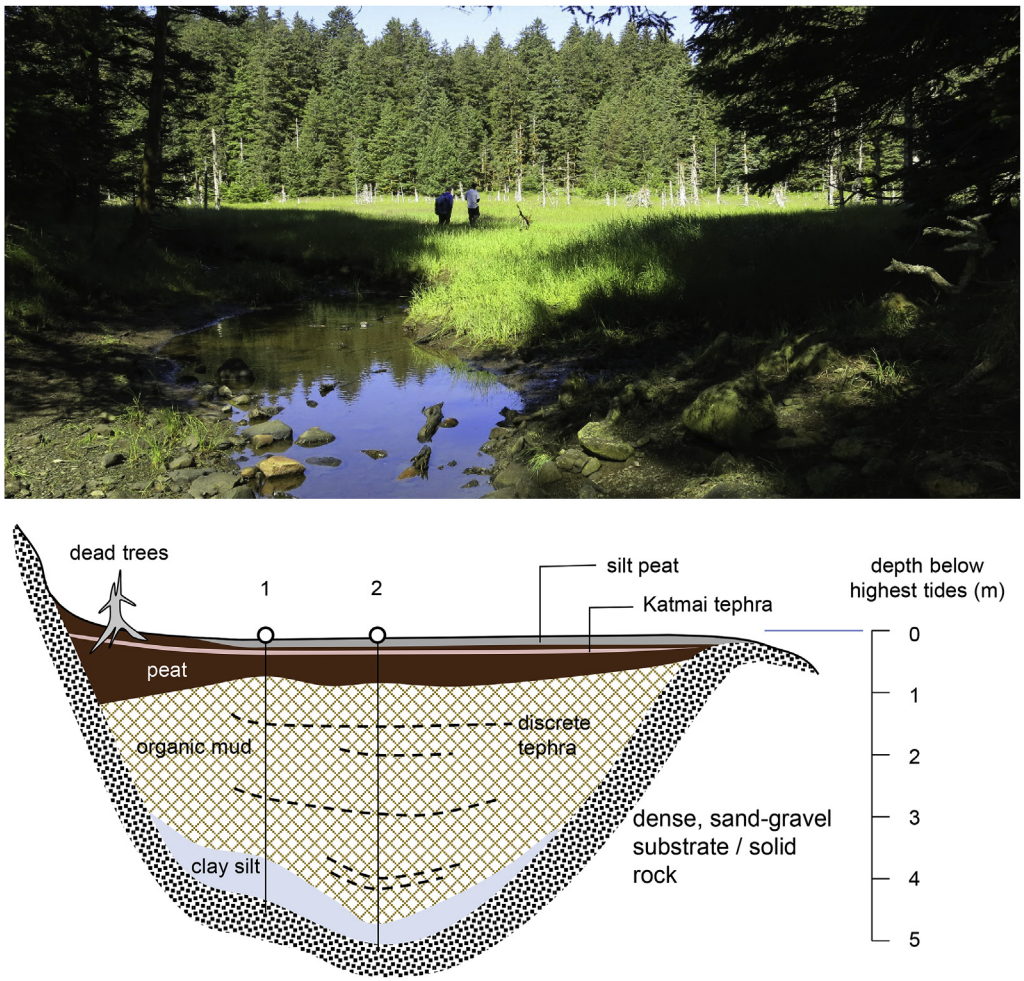

Fig. 12. Photograph of South Carry Inlet Marsh, looking WNW into the marsh from the connection to South Carry Inlet, and schematic section derived from two cores, tidal creek exposures, surface morphology and vegetation.

will judge the evidence from Shuyak against the well-accepted criteria, originally proposed with respect to tidal marsh sequences adjacent to the Cascadia subduction zone (Nelson et al., 1996), and successfully applied elsewhere with some additions, to distinguish sediment couplets that result from great earthquake subsidence or emergence from those produced by other processes (Shennan et al., 2016). These criteria are, 1 - lateral extent of peat-mud or mud-peat couplets, or other changes in sediment stratigraphy indicating rapid submergence or emergence; 2 - suddenness of submergence or emergence, indicated by sharp, < 1 mm, or abrupt, <3 mm contacts; 3 - amount of vertical motion; 4 - presence of tsunami deposited sediments directly above the peat horizon; 5 - synchroneity with other sites, and 6, the spatial pattern of submergence and emergence for each proposed earthquake. Previous coastal paleoseismic studies in Alaska that successfully used these criteria mostly describe locations where the marshes are much larger than those on Shuyak, and where there is an abundant supply of fine-grain sediment to the intertidal zone. The marshes on Shuyak are small, most <100 m across on their smallest axis, with limited silt and clay-size minerogenic sediment input which contributes to the discontinuous nature of minerogenic post-subsidence deposits, making correlation between sites less straightforward.

The sedimentary record of the 1964 earthquake provides a valuable analogue for assessing any previous earthquakes. Plafker (1969) reports ~1.05 m subsidence in 1964, based on a temporary tidal benchmark at Carry Inlet (Fig. 3). A change in sediment stratigraphy at all our field locations records marsh submergence but the clarity varies. In some exposures, we see evidence of sediment reworking and sediment mixing at the contact and therefore the sharpness of the contact differs laterally over short distances. Even where it is sharp and clear, such as the outcrop at Skiff Passage Marsh, the diatom reconstruction indicates ~0.3 m submergence (Figs. 10 and 11). The difference could all be due to a sediment hiatus, but we suggest that this may also result from a combination of low sediment input and rapid post-seismic uplift. Following ~1.7 m coseismic subsidence, rapid uplift at the tide station on Kodiak Island totalled 0.47 ± 0.08 m during a 3.5 year period starting mid-1964 (Larsen et al., 2003). Remeasurement of the tidal benchmark at Carry Inlet indicated 0.45 m post-seismic uplift in 39 years (Gilpin, 1995). Nevertheless, the 0.3 m diatom-based estimate for subsidence in 1964 is greater than the elevation changes estimated, using the same method, for all the possible earlier earthquake event horizons described from Bear Trail Marsh, Deer Marsh and Skiff Passage Marsh.

One further process compounds the difficulty of identifying coseismic submergence. We see abundant evidence of sediment reworking by winter sea ice. Blocks of sediment become frozen to the ice, detached, transported and deposited at a different elevation. This is a common process on Alaskan marshes and can lead to

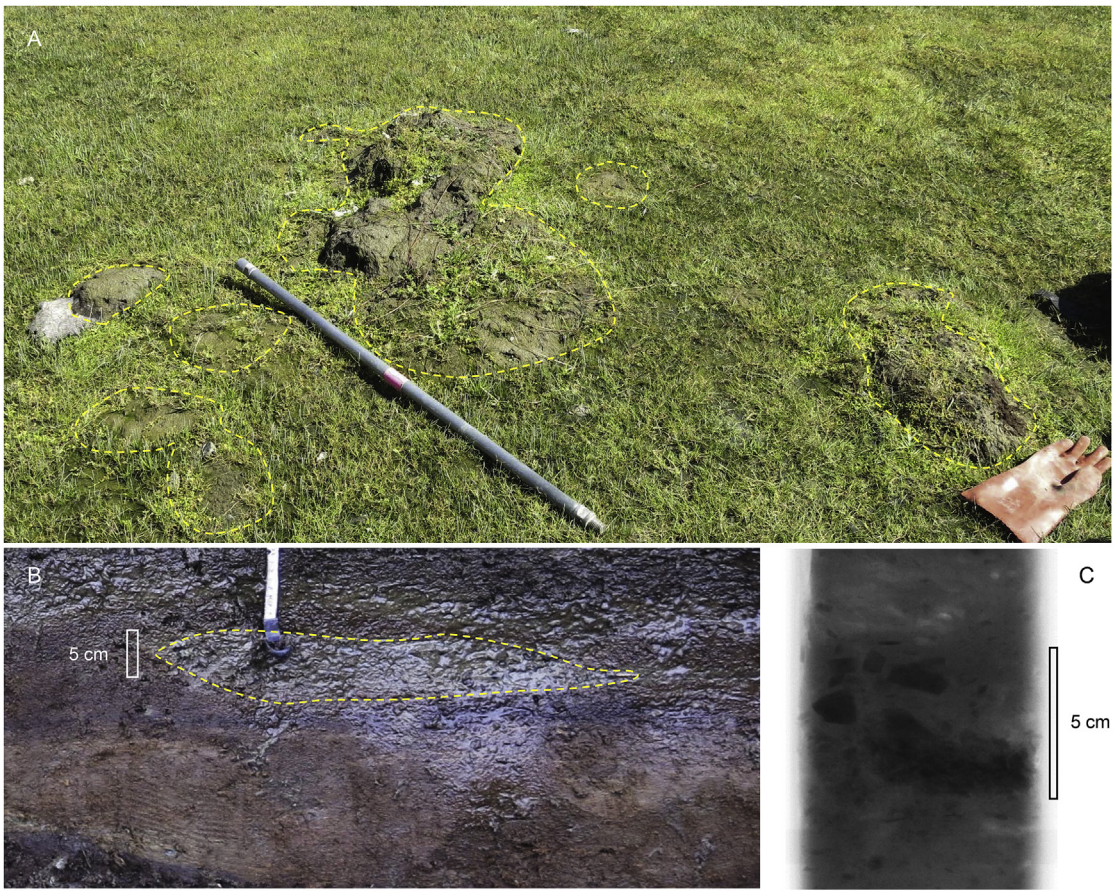

Fig. 13. Evidence of ice rafting, A) on the marsh surface (yellow dashes) at Bear Trail Marsh, metal pole = 1 m; B) in outcrop (yellow dashes) at Skiff Passage Marsh; C) X-ray, from 39 to 49 cm depth, across the sand/gravel lens in the Bear Trail Marsh outcrop (Fig. 5). (For interpretation of the references to colour in this figure legend, the reader is referred to the Web version of this article.)

lenses of minerogenic sediment, of all size ranges from clay to coarse gravel, within predominantly peat units, or lenses of peat within minerogenic units. Individual sediment blocks may be > 1 m in length although the majority are smaller (Hamilton et al., 2005). There is widespread evidence of sediment reworked in this fashion on the Shuyak marshes (Fig. 13).

Given the evidence described above, for only decimeter-scale abrupt changes in elevation and post-depositional processes that may blur the sedimentary record of coseismic submergence or emergence, interpretations require close consideration of evidence of absence of rapid emergence or submergence versus absence of evidence. Our working hypotheses will therefore consider the evidence over the last 2000 years, the maximum length of the records from Deer Marsh, Bear Trial Marsh and Skiff Passage Marsh, during which time there is evidence from other locations of great earthquakes prior to AD 1964. These are AD 1788, recorded in documentary and sedimentary evidence (Briggs et al., 2014; Shennan et al., 2014a; Soloviev, 1990; Witter et al., 2014), a Kodiak segment-only earthquake c.500 BP (Carver and Plafker, 2008; Gilpin, 1995; McCalpin and Carver, 2009), two earthquakes recorded in the Prince William Sound (PWS) segment, PWS-1 c.850 BP and PWS-2 c.1500 BP (Carver and Plafker, 2008; Kelsey et al., 2015; Shennan et al., 2014b), and an earthquake in SE Kenai between PWS-1 and AD 1964 (Kelsey et al., 2015).

For each of these four earthquakes we test three alternative hypotheses: 1) evidence of no abrupt change; 2) evidence of abrupt change; 3) no evidence. Table 2 summarises our evidence from Bear Trail Marsh, Deer Marsh and Skiff Passage Marsh against the Nelson et al. (1996) criteria. These range from changes in sediment stratigraphy with sharp contacts and a degree of lateral continuity, to evidence of no change in sediment stratigraphy at the time of a proposed earthquake. The final data to consider come from the previously noted change in peat stratigraphy at Bear Trail Marsh.

We see contradictory evidence from Shuyak with respect to the age of the proposed c.500 BP earthquake. Skiff Passage Marsh has a long hiatus. Deer Marsh has a peat-mud couplet and diatom evidence of submergence, but at c.400 BP rather than c.500 BP, well-constrained by the age model based on dated samples at ~4 cm intervals. Bear Trail Marsh has a sand/gravel layer dated earlier, 566 ± 36 BP, with no evidence of elevation change.

In contrast, a few centimetres up-section, a gradual change in peat stratigraphy records submergence at c.400 BP (Figs. 4 and 5, Table 2). Previous investigations of the stratigraphic evidence of coseismic submergence in AD 1964 on the Kenai peninsula (Fig. 1) show how changes in peat stratigraphy in a more landward part of the marsh can record submergence. These changes grade spatially to a clear peat-silt boundary further seaward (Hamilton and Shennan, 2005b; Zong et al., 2003). The change in peat stratigraphy at Bear Trail Marsh is visible across outcrop 8 and in core 2. It could also correlate with a thin minerogenic layer in outcrop 7, further seaward (Fig. 4). Therefore, in testing for synchroneity between sites we will also consider this horizon as a possible record of coseismic submergence.

Table 2
Summary of evidence from Bear Trail Marsh, Deer Marsh and Skiff Passage Marsh for four previously proposed earthquakes in the last 2000 years.

	PWS-2 c.1500BP	PWS-1 c.850 BP	Kodiak c.500/400 BP		AD 1788
Bear Trail Marsh					
Contact depth	No change in stratigraphy	No change in stratigraphy	66.5 cm	59 cm – change in peat colour	38.5 cm
Contact sharpness			<1 mm	>10 mm	<1 mm
Lateral extent			<25 m?	>25 m	>100 m
Elevation change – both models			None	−0.33 ± 0.50 m LW-WA −0.44 ± 0.57 m WAPLS	−0.13 ± 0.50 m LW-WA −0.27 ± 0.57 m WAPLS
Tsunami sediment			Possible – sand/gravel	None	None
Age model estimate			566 ± 36 BP	440 to 387 ± 25 BP	AD 1788
Deer Marsh					
Contact depth	Beyond age range of outcrop	Beyond age range of outcrop	88 cm		41 cm
Contact sharpness			<1 mm		<1 mm
Lateral extent			3 outcrops		3 outcrops
Elevation change – both models			−0.19 ± 0.50 m LW-WA −0.31 ± 0.58 m WAPLS		+0.01 ± 0.41 m LW-WA −0.16 ± 0.57 m WAPLS
Tsunami sediment			None		None
Age model estimate			390 ± 75 BP		AD 1788
Skiff Passage Marsh					
Contact depth	Beyond age range of outcrop	120 cm	103 cm		23.5 cm
Contact sharpness		<1 mm	<1 mm		<1 mm
Lateral extent		One outcrop	One outcrop		One outcrop
Elevation change – both models		+0.01 ± 0.47 m LW-WA −0.08 ± 0.58 m WAPLS	+0.68 ± 0.59 m LW-WA across hiatus +0.62 ± 0.46 m WAPLS across hiatus		−0.03 ± 0.41 m LW-WA −0.09 ± 0.56 m WAPLS
Tsunami sediment		None	Possible – silt/sand/gravel		None
Age model estimate		Hiatus from 995 ± 60 to 687 ± 14 BP	Hiatus from 682 ± 11 to 213 ± 50 BP		AD 1788

5.2. Extent of coseismic deformation during Late Holocene earthquakes

Recent paleoseismological data from Kodiak Island and an analysis of radiocarbon data based on Bayesian age modelling gave a wider age range for the proposed c.500 BP earthquake, 510 - 330 BP (Shennan et al., 2014a), than previously suggested, 533 - 473 BP (Carver and Plafker, 2008). The new data from Shuyak Island (Table 2) seem more compatible with an age in the younger part of the wider range, c.400 BP, assuming it is the same, single event being recorded at each marsh.

New radiocarbon data from Sitkinak Island (Briggs et al., 2014) together with those from Shuyak Island described above provide much better controls on the modelled ages of earthquake than those available from the earlier Bayesian models and help resolve some of the previously encountered issues (Shennan et al., 2014a). When including all the radiocarbon data from the whole Kodiak segment the earlier models found no numerical convergence and therefore no acceptable fit, and thus used separate models for two sub-regions, Shuyak Island in one and SE Kodiak Island in another (Shennan et al., 2014a). Here we return to asses a single model that incorporates the whole of the Kodiak archipelago. We adopt the same Bayesian approach, grouping samples into “phases” between proposed earthquakes, whether they are minimum or maximum ages for the proposed earthquakes (Bronk Ramsey, 2009; Lienkaemper and Bronk Ramsey, 2009). The data available from Sitkinak Island, Shuyak Island and Kodiak Island provide better stratigraphic control and so allow us to exclude samples with poor or no evidence of the lateral extent of a contact within an individual marsh (c.f. Shennan et al., 2014a).

Our new model combines first the data from marsh sediment sequences Sitkinak Island, Shuyak Island and SE Kodiak Island (Supplementary file). We then add marsh and archaeological data of tsunami inundation of middens and houses on Afognak Island (Carver and Plafker, 2008; Clark, 2005, 2008). The well-documented radiocarbon plateau from c.AD 1700 to modern provides a challenge in determining the age of any event within this period. This period includes the likely age for the peat-silt couplet recorded at many sites a few centimeters below the Katmai tephra of AD 1912. Therefore we run an unconstrained model for this peat-silt couplet and a second model where we define the age of the couplet as AD 1788, correlating the geological evidence with historical records of ground shaking, a tsunami and net submergence (Soloviev, 1990). Finally, we compare the modelled ages from the Kodiak segment with those from the Prince William Sound segment (Fig. 14).

Correlating the results of the age model at sites across the Kodiak archipelago with the stratigraphic evidence for coseismic vertical deformation reveals subtle differences in the pattern of deformation (Fig. 15). The extent, timing and amount of deformation (Table 2, Figs. 13 and 14) all contrast with the present seismic hazard maps for Alaska which adopt characteristic earthquakes for the AD 1964 rupture zone (Fig. 1), as M_w 9.2 every 650 years, and for the Kodiak segment alone, as M_w 8.8 every 650 years.

In terms of coseismic elevation change, our evidence indicate less change in all cases, at the scale of a few decimetres compared to ~1 m in previous studies (Gilpin, 1995; Gilpin et al., 1994; McCalpin and Carver, 2009). We have previously noted the low input of clastic sediment into the marshes on Shuyak Island, rapid post-seismic recovery, and reworking of sediment by winter sea ice. In combination these factors will likely result in an underestimate of subsidence using diatom-based transfer functions across peat-silt contacts, as the 0.5 cm thick sample of silt used for analysis from above a contact contains a mix of diatom assemblages deposited

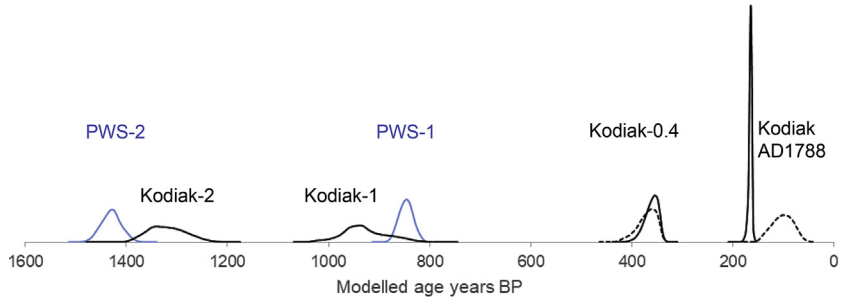

Fig. 14. 95% probability density functions of modelled ages for earthquakes for the Kodiak segment (Details in supplementary files) and the Prince William Sound segment (Shennan et al., 2016). For Kodiak-0.4, broken line = marsh sediment data only, solid line includes archaeological data from Afognak Island; for AD 1788, dashed line = unconstrained modelled age, solid line = model constrained by documentary evidence.

over a number of years, with the potential for a possible sedimentation hiatus and also possible sediment reworking. We could, therefore, take our decimetre-scale estimates of submergence (Table 2) as indicating ~1 m subsidence, as in AD 1964. We note, however, that the in-field stratigraphic evidence of submergence in AD 1964 is recorded more clearly at all Shuyak sites than any of the earlier events, especially in terms of the lateral continuity across each marsh. As a result our decimetre-scale estimate of submergence during the earlier events, while still an underestimate, reflects less subsidence than in AD 1964. We also note that changes in peat stratigraphy alone can record submergence, in one case in the order of 0.4 m (Fig. 6 and Table 2), but other examples show no elevation change across peat to peat contacts (Figs. 9 and 11).

The modelled ages (Fig. 14) contrast with previous estimates (Carver and Plafker, 2008; Shennan et al., 2014a) in two respects. First, the earthquake originally dated 533–473 BP, now has a modelled age of 440–320 BP. This age range is constrained by our new data from Shuyak, those from Middle Bay, Kalsin Bay and Anton Larson Bay on Kodiak Island (Shennan et al., 2014a, 2016), Afognak River and Settlement Point on Afognak Island (Carver and Plafker, 2008; Clark, 2005, 2008), and Sitkinak Island (Briggs et al., 2014). Second, the correlation and synchroneity with earthquakes in the Prince William Sound segment, c.850 BP and c.1500 BP, is equivocal. Our new data from Shuyak show evidence of no coseismic elevation change at Bear Trail Marsh for either event, no evidence in the required age range at Deer Marsh, and a long hiatus at Skiff Passage Marsh (Table 2). There is no evidence for rapid submergence at either time at both Anton Larson Bay and Kalsin Bay, where records extend back to pre-2000 BP. The most stringent age constraint for earthquakes c. 850 BP and c. 1500 BP in the Kodiak segment is for the younger event, from two radiocarbon ages bracketing a tsunami sand at the Afognak River archaeological site (Carver and Plafker, 2008; Clark, 2005, 2008). We suggest that the data base of radiocarbon ages is too small from the Kodiak segment to conclude whether, based on age modelling alone, earthquakes in the Prince William Sound segment c.850 BP and c.1500 BP correlate with the Kodiak paleoseismic evidence, suggesting multi-segment ruptures, or whether there were single segment ruptures a few years or decades apart.

5.3. The persistence, or non-persistence of rupture boundaries

The spatial pattern of coseismic deformation helps to constrain rupture boundaries and differentiate between single segment and

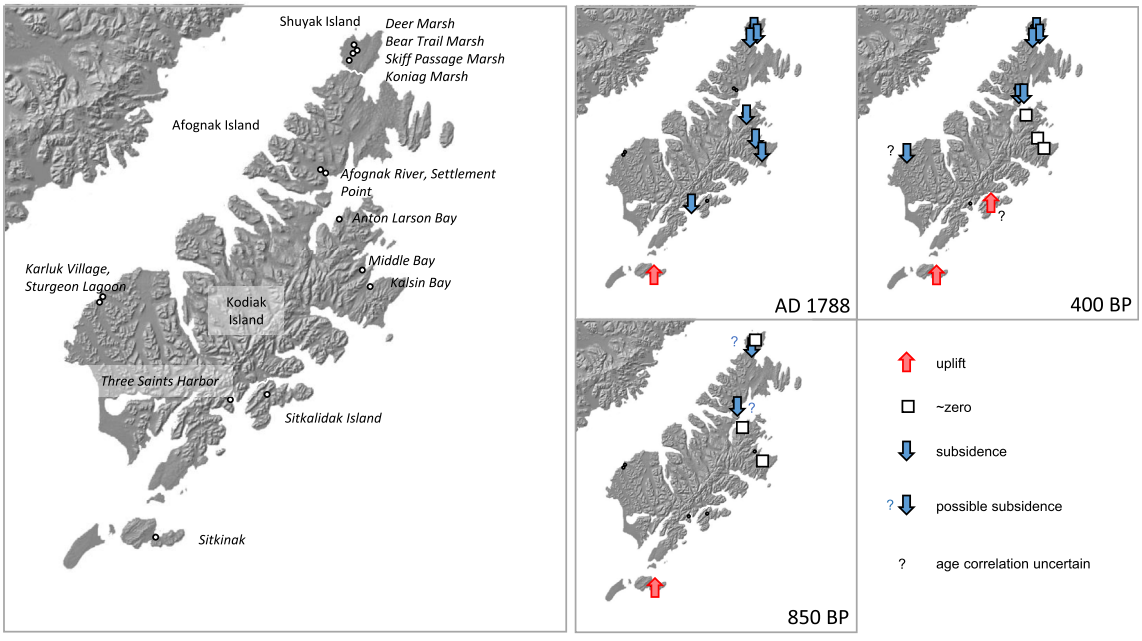

Fig. 15. Summary of coseismic land motion, AD 1788, c.400 BP and c.850 BP. Relative ground motions are inferred from sediment stratigraphy and microfossil analyses where present and, for Three Saints Harbor, historical accounts.

multi-segment ruptures. The patterns of coseismic deformation across the Kodiak archipelago differ slightly for three pre-1964 earthquakes (Fig. 15). Uplift in Sitkinak and subsidence in SE Kodiak Island fits well with the model of a single segment M_w8.0 earthquake (Case C from Suleimani et al., 2017) with slip on the plate interface between 30 and 10 km depth (Fig. 2), however coseismic subsidence extending to Shuyak Island during a M_w8.0 earthquake requires slip occurring to perhaps 40 km. In contrast, a single segment M_w 9.1 earthquake model, with maximum slip at 10 km and updip and downdip limits of the rupture at 1 and 35 km (Scenario 2 from Suleimani et al., 2017), produces subsidence on Shuyak Island and across SE Kodiak Island, but the predictions of subsidence, ~1.5 m on Shuyak and ~2.2 m in SE Kodiak, are much greater than the estimates from our diatom-based transfer functions. Further modelling would produce tighter constraints on possible rupture patterns, nonetheless these earthquake models illustrate a range of possible scenarios of single segment ruptures which encompass the patterns shown in Fig. 15.

Single Kodiak segment scenarios fit with interpretations of evidence from the Kenai peninsula that the c.850 BP and c.1500 BP earthquakes were ruptures of the Prince William Sound segment together with part of the Kenai segment (Shennan et al., 2016). This interpretation assumes that there exists a roughly correct framework of major ruptures along this stretch of the subduction zone within the scenarios of regional modelling studies (Nicolsky et al., 2013, 2014; Suleimani et al., 2002, 2017). None of the modelled scenarios predict deformation extending across the Kodiak, Kenai and Prince William Sound segments without deformation extending to key sites in those segments, around Cook Inlet and Copper River Delta (Locations 10–12 and 14–18 in Fig. 1). The pattern and extent of deformation c.850 BP and c.1500 BP recorded at these sites (Shennan et al., 2016), and at SE Kenai c.850 BP (Kelsey et al., 2015), fit closely to rupture scenarios comprising the Prince William Sound segment and part of the Kenai segment, generating M_w 8.8 earthquakes (Shennan et al., 2016).

Evidence from SE Kenai (location 13 in Fig. 1) indicates deformation near the boundary between the Prince William Sound and Kenai segments on one further occasion before AD 1964 (Kelsey et al., 2015). The radiocarbon evidence mean it could be correlated with either the Kodiak AD 1788 or c.400 BP earthquake, or it could be independent of both. Sites in the Kenai segment along Cook Inlet (Locations, 10–12 in Fig. 1) however, have either no evidence of coseismic deformation or evidence indicating no coseismic deformation at AD 1788 and c.400 BP (Shennan et al., 2016). Further modelling is required of possible rupture patterns to test the correlation or independence of this earthquake recorded at SE Kenai.

In terms of seismic hazard assessment, our interpretations of the paleoseismic evidence and the scenarios of coseismic deformation indicate (1) in the last 2000 years AD 1964 was the only earthquake, M_W 9.2, to rupture from the Prince William Sound segment, across the Kenai segment, to the Kodiak segment, and (2) the Kodiak segment ruptured independently on four further occasions, with earthquakes > M_W 8.0; in AD 1788, c.400 BP, and independently but around the times of great earthquakes in the Prince William Sound segment c.850 and c.1500 BP.

We also note the absence of an earthquake producing a record of marsh submergence or emergence across the Kodiak archipelago in the period from c.800 to c.400 BP (Fig. 14). In contrast to uplift on Sitkinak Island in 1788, c.400 BP and c.850 BP, Briggs et al. (2014) record coseismic submergence at the same location c.600 BP, implying a different pattern of rupture to the other earthquakes recorded in the marshes on Kodiak Island, Afognak Island and Shuyak Island.

6. Conclusions

Sediment sequences from tidal marshes in Shuyak Island provide evidence of past earthquakes during the last 2000 years. Low sediment supply, rapid post-seismic uplift and sediment reworking by winter sea ice hinder the preservation of paleoseismic evidence but closely-spaced radiocarbon samples through individual sections provide age models to help identify sediment hiatuses and periods of continuous sedimentation. These chronologies, alongside estimates of marsh elevation changes from diatom-based transfer function models, allow us to consider evidence of no land-level change, in contrast to absence of evidence, when testing alternative hypotheses regarding the amount, extent and age of coseismic deformation. When combined with evidence from the Kodiak, Kenai and Prince William Sound segments, the paleoseismic history inferred here from Shuyak Island shows different patterns of rupture during the last 2000 years that can be incorporated into models for the purposes of seismic hazard analysis.

Credit authorship contribution

IS: devised the project, undertook fieldwork and data analyses, and led the writing of the paper; all authors commented on the paper and approved the final article. In addition, **MDB:** contributed to project formulation, undertook fieldwork, diatom analyses and data analyses. **NLMB:** contributed to project formulation and data analyses. **FPD:** undertook fieldwork and laboratory analyses. **CL and NT:** undertook laboratory analyses.

Declarations of interest

None.

Acknowledgements

The project described in this publication is based upon work supported by NERC (Radiocarbon Award 2051.0317) and the United States Geological Survey under Grant/Cooperative Agreement Number (G16AP00112). Rich Briggs and Harvey Kelsey provided highly valuable reviews. The views and conclusions contained in this document are those of the authors and should not be interpreted as representing the opinions or policies of the U.S. Geological Survey. Mention of trade names or commercial products does not constitute their endorsement by the U.S. Geological Survey.

Appendix A. Supplementary data

Supplementary data related to this article can be found at https://doi.org/10.1016/j.quascirev.2018.10.028.

Supplementary files contain: 1) diatom data; 2) Geochemical/XRF data; 3) radiocarbon data used to model earthquake ages; 4) earthquake age model output.

References

Briggs, R.W., Engelhart, S.E., Nelson, A.R., Dura, T., Kemp, A.C., Haeussler, P.J., Corbett, D.R., Angster, S.J., Bradley, L.-A., 2014. Uplift and Subsidence Reveal a Nonpersistent Megathrust Rupture Boundary (Sitkinak Island, Alaska). Geophysical Research Letters, 2014GL059380.

Bronk Ramsey, C., 2001. Development of the radiocarbon calibration program. Radiocarbon 43, 355–363.

Bronk Ramsey, C., 2008. Deposition models for chronological records. Quat. Sci. Rev. 27, 42–60.

Bronk Ramsey, C., 2009. Bayesian analysis of radiocarbon dates. Radiocarbon 51, 337–360.

Butler, R., 2012. Re-examination of the potential for great earthquakes along the aleutian island arc with implications for tsunamis in Hawaii. Seismol Res. Lett. 83, 29–38.

Carver, G., Plafker, G., 2008. Paleoseismicity and neotectonics of the aleutian subduction zone - an overview. In: Freymueller, J.T., Haeussler, P.J., Wesson, R., Ekstrom, G. (Eds.), Active Tectonics and Seismic Potential of Alaska. American Geophysical Union, Washington, pp. 43–63.
Cisternas, M., Garrett, E., Wesson, R., Dura, T., Ely, L.L., 2017. Unusual geologic evidence of coeval seismic shaking and tsunamis shows variability in earthquake size and recurrence in the area of the giant 1960 Chile earthquake. Mar. Geol. 385, 101–113.
Clark, D., 2005. Ancient Afognak: precontact history and archaeology of Afognak bay. http://www.afognak.org/heritage/history/history-intro.php?src=ancient-afognak. (Accessed 18 January 2018).
Clark, D.W., 2008. Five seasons with the late kachemak. Alaska J. Anthropol. 6, 185–197.
Dura, T., Cisternas, M., Horton, B.P., Ely, L.L., Nelson, A.R., Wesson, R.L., Pilarczyk, J.E., 2015. Coastal evidence for Holocene subduction-zone earthquakes and tsunamis in central Chile. Quat. Sci. Rev. 113, 93–111.
Dura, T., Hemphill-Haley, E., Sawai, Y., Horton, B.P., 2016. The application of diatoms to reconstruct the history of subduction zone earthquakes and tsunamis. Earth Sci. Rev. 152, 181–197.
Freymueller, J.T., Woodard, H., Cohen, S.C., Cross, R., Elliott, J., Larsen, C.F., Hreinsd, oacute, ttir, S., Zweck, C., 2008. Active deformation processes in Alaska, based on 15 years of GPS measurements. In: Freymueller, J.T., Haeussler, P.J., Wesson, R., Ekström, G. (Eds.), Active Tectonics and Seismic Potential of Alaska. AGU, Washington, DC, pp. 1–42.
Garrett, E., Shennan, I., Woodroffe, S.A., Cisternas, M., Hocking, E.P., Gulliver, P., 2015. Reconstructing paleoseismic deformation, 2: 1000 years of great earthquakes at Chucalén, south central Chile. Quat. Sci. Rev. 113, 112–122.
Gilpin, L.M., 1995. Holocene Paleoseismicity and Coastal Tectonics of the Kodiak Islands, Alaska. University of California, Santa Cruz, Santa Cruz, p. 358.
Gilpin, L.M., Ward, S., Anderson, R., Moore, J.C., Carver, G., 1994. Holocene Interseismic Deformation and Stratigraphic Modelling of the Earthquake Cycle, Kodiak Islands, Alaska, pp. 339–344. USGS Open File Report 94 - 176.
Hamilton, S., Shennan, I., 2005a. Late Holocene relative sea-level changes and the earthquake deformation cycle around upper Cook Inlet, Alaska. Quat. Sci. Rev. 24, 1479–1498.
Hamilton, S., Shennan, I., Combellick, R., Mulholland, J., Noble, C., 2005. Evidence for two great earthquakes at Anchorage, Alaska and implications for multiple great earthquakes through the Holocene. Quat. Sci. Rev. 24, 2050–2068.
Hamilton, S.L., Shennan, I., 2005b. Late Holocene great earthquakes and relative sea-level change at Kenai, southern Alaska. J. Quat. Sci. 20, 95–111.
Hildreth, W., 1983. The compositionally zoned eruption of 1912 in the valley of ten thousand smokes, Katmai national park, Alaska. J. Volcanol. Geoth. Res. 18, 1–56.
Juggins, S., 2014. C2 Version 1.7.6. Newcastle University, Newcastle upon Tyne. https://www.staff.ncl.ac.uk/stephen.juggins/software/C2Home.htm.
Kelsey, H.M., Witter, R.C., Engelhart, S.E., Briggs, R., Nelson, A., Haeussler, P., Corbett, D.R., 2015. Beach ridges as paleoseismic indicators of abrupt coastal subsidence during subduction zone earthquakes, and implications for Alaska-Aleutian subduction zone paleoseismology, southeast coast of the Kenai Peninsula, Alaska. Quat. Sci. Rev. 113, 147–158.
Kemp, A.C., Telford, R.J., 2015. Transfer functions. In: Shennan, I., Long, A.J., Horton, B.P. (Eds.), Handbook of Sea-level Research. AGU John Wiley & Sons, Ltd, pp. 470–499.
Kirby, S., Scholl, D.,W., von Huene, R., Wells, R.,E., 2013. Alaska Earthquake Source for the SAFRR Tsunami Scenario. U.S. Geological Survey Open-File Report 2013-1170-B, p. 40.
Larsen, C.F., Echelmeyer, K.A., Freymueller, J.T., Motyka, R.J., 2003. Tide gauge records of uplift along the northern Pacific-North American plate boundary, 1937 to 2001. J. Geophys. Res.: Solid Earth 108, 2216.
Lienkaemper, J.J., Bronk Ramsey, C., 2009. OxCal: versatile tool for developing paleoearthquake chronolgies - a primer. Seismol Res. Lett. 80, 431–434.
McCalpin, J.,P., Carver, G., 2009. Paleoseismology of compressional tectonic environments. In: McCalpin, J.,P. (Ed.), Paleoseismology, second ed. Academic Press, Burlington, pp. 315–419.
Mueller, C.S., Briggs, R.W., Wesson, R.L., Petersen, M.D., 2015. Updating the USGS seismic hazard maps for Alaska. Quat. Sci. Rev. 113, 39–47.
Nelson, A.R., Briggs, R.W., Dura, T., Engelhart, S.E., Gelfenbaum, G., Bradley, L.-A., Forman, S.L., Vane, C.H., Kelley, K.A., 2015. Tsunami recurrence in the eastern Alaska-Aleutian arc: a Holocene stratigraphic record from Chirikof Island, Alaska. Geosphere 11, 1172–1203.
Nelson, A.R., Shennan, I., Long, A.J., 1996. Identifying coseismic subsidence in tidal-wetland stratigraphic sequences at the Cascadia subduction zone of western North America. J. Geophys. Res. 101, 6115–6135.
Nicolsky, D.J., Suleimani, E.N., Haeussler, P.J., Ryan, H.F., Koehler, R.D., Combellick, R.A., Hansen, R.A., 2013. Tsunami Inundation Maps of Port Valdez, Alaska. Alaska Division of Geological & Geophysical Surveys Report of Investigation 2013-1, pp. 1–77.
Nicolsky, D.J., Suleimani, E.N., Koehler, R.D., 2014. Tsunami Inundation Maps of Cordova and Tatitlek, Alaska. Alaska Division of Geological & Geophysical Surveys Report of Investigation 2014-1, pp. 1–49.
NOAA, 2016. Tides and Currents. Silver Spring, MD, USA. https://tidesandcurrents.noaa.gov/products.html. p. Center for Operational Oceanographic Products and Services.
Plafker, G., 1969. Tectonics of the March 27, 1964, Alaska Earthquake. U.S. Geological Survey Professional Paper 543-I, p. 74.
Plafker, G., Kachadoorian, R., 1966. Geologic Effects of the March 1964 Earthquake and Associated Seismic Sea Waves on Kodiak and Nearby Islands, Alaska. U.S. Geological Survey Professional Paper 543-D, p. 46.
Reger, R.D., Sturmann, A.G., Berg, E.E., Burns, P.A.C., 2007. State of Alaska Department of Natural Resources, Division of Geological & Geophysical Surveys Guidebook. A Guide to the Late Quaternary History of Northern and Western Kenai Peninsula, Alaska, vol. 8, pp. 1–112.
Ryan, H.,F., von Huene, R., Wells, R.,E., Scholl, D.,W., Kirby, S., Draut, A.,E., 2012. History of Earthquakes and Tsunamis along the Eastern Aleutian-Alaska Megathrust, with Implications for Tsunami Hazards in the California Continental Borderland. U.S. Geological Survey Professional Paper 1795-A, p. 31.
SAFFR, 2013. (Science Application for Risk Reduction) Tsunami Modeling Working Group: Modeling for the SAFRR Tsunami Scenario-generation, Propagation, Inundation, and Currents in Ports and Harbors. U.S. Geological Survey Open-File Report 2013-1170-D, p. 136.
Sawai, Y., Satake, K., Kamataki, T., Nasu, H., Shishikura, M., Atwater, B.F., Horton, B.P., Kelsey, H.M., Nagumo, T., Yamaguchi, M., 2004. Transient uplift after a 17th-Century earthquake along the Kuril subduction zone. Science 306, 1918–1920.
Shennan, I., 2009. Late Quaternary sea-level changes and palaeoseismology of the Bering Glacier region, Alaska. Quat. Sci. Rev. 28, 1762–1773.
Shennan, I., Barlow, N., Combellick, R., 2008. Paleoseismological records of multiple great earthquakes in southcentral Alaska: a 4000-year record at Girdwood. In: Freymueller, J.T., Haeussler, P.J., Wesson, R., Ekström, G. (Eds.), Active Tectonics and Seismic Potential of Alaska. AGU, Washington, DC, pp. 185–199.
Shennan, I., Barlow, N.L.M., Brader, M., 2017. Late Holocene Paleoseismology and Plate Segmentation of the Alaska 1964 Rupture Zone. Final Report USGS External Grant Award # G16AP00112.
Shennan, I., Barlow, N.L.M., Carver, G., Davies, F., Garrett, E., Hocking, E., 2014a. Great tsunamigenic earthquakes during the past 1000 yr on the Alaska megathrust. Geology 42, 687–690.
Shennan, I., Barlow, N.L.M., Combellick, R., Pierre, K., Stuart-Taylor, O., 2014b. Late Holocene paleoseismology of a site in the region of maximum subsidence during the 1964 Mw 9.2 Alaska earthquake. J. Quat. Sci. 29, 343–350.
Shennan, I., Bruhn, R., Barlow, N.L.M., Good, K., Hocking, E., 2014c. Late Holocene great earthquakes in the eastern part of the Aleutian megathrust. Quat. Sci. Rev. 84, 86–97.
Shennan, I., Bruhn, R., Plafker, G., 2009. Multi-segment earthquakes and tsunami potential of the Aleutian megathrust. Quat. Sci. Rev. 28, 7–13.
Shennan, I., Garrett, E., Barlow, N.L.M., 2016. Detection limits of tidal-wetland sequences to identify variable rupture modes of megathrust earthquakes. Quat. Sci. Rev. 150, 1–30.
Shennan, I., Hamilton, S.L., 2010. Holocene sea-level changes and earthquakes around Bering Glacier. In: Shuchman, R., Josberger, E., Jenkins, L. (Eds.), Bering Glacier: Interdisciplinary Studies of Earth's Largest Temperate Surging Glacier: Geological Society of America Special Paper 462. Geological Society of America, Boulder, pp. 275–290.
Soloviev, S.L., 1990. Sanak-Kodiak tsunami of 1788. Sci. Tsunami Hazards 8, 34-30.
Stuiver, M., Reimer, P.J., Reimer, R., 2017. CALIB Radiocarbon Calibration 7.1 [WWW program] at. http://calib.org. downloaded 2017-08-11.
Suleimani, E.N., Hansen, R.A., Combellick, R.A., Carver, G.A., Kamphaus, R.A., Newman, J.C., Venturato, A.J., 2002. Tsunami Hazard Maps of the Kodiak Area, Alaska. Alaska Division of Geological & Geophysical Surveys Report of Investigation 2002-1, pp. 1–16.
Suleimani, E.N., Nicolsky, D.J., Koehler, R.D., 2017. Updated Tsunami Inundation Maps of the Kodiak Area, Alaska. Alaska Division of Geological & Geophysical Surveys Report of Investigation 2017-8, p. 38, 10 sheets.
Watcham, E.P., Shennan, I., Barlow, N.L.M., 2013. Scale considerations in using diatoms as indicators of sea-level change: lessons from Alaska. J. Quat. Sci. 28, 165–179.
Wesson, R.L., Boyd, O.S., Mueller, C.S., Bufe, C.G., Frankel, A.D., Petersen, M.D., 2007. Revision of Time-independent Probabilistic Seismic Hazard Maps for Alaska. U.S. Geological Survey Open-File Report, pp. 1–33.
Wesson, R.L., Boyd, O.S., Mueller, C.S., Frankel, A.D., 2008. Challenges in making a seismic hazard map for Alaska and the Aleutians. In: Freymueller, J.T., Haeussler, P.J., Wesson, R., Ekström, G. (Eds.), Active Tectonics and Seismic Potential of Alaska. AGU, Washington, DC, pp. 385–397.
West, C.F., 2011. A revised radiocarbon sequence for Karluk-1 and the implications for Kodiak Island prehistory. Arctic Anthropol. 48, 80–92.
Witter, R.C., Briggs, R.W., Engelhart, S.E., Gelfenbaum, G., Koehler, R.D., Barnhart, W.D., 2014. Little Late Holocene Strain Accumulation and Release on the Aleutian Megathrust below the Shumagin Islands, Alaska. Geophysical Research Letters, 2014GL059393.
Zong, Y., Shennan, I., Combellick, R.A., Hamilton, S.L., Rutherford, M.M., 2003. Microfossil evidence for land movements associated with the AD 1964 Alaska earthquake. Holocene 13, 7–20.